

# Concentration quenching, surface and spectral analyses of SrF<sub>2</sub>:Pr<sup>3+</sup> prepared by different synthesis techniques



M.Y.A. Yagoub, H.C. Swart, E. Coetsee\*

Department of Physics, University of the Free State, PO Box 339, Bloemfontein ZA9300, South Africa

## ARTICLE INFO

### Article history:

Received 4 September 2014  
Received in revised form 10 January 2015  
Accepted 12 January 2015  
Available online 7 February 2015

### Keywords:

SrF<sub>2</sub>:Pr<sup>3+</sup>  
Concentration quenching  
XPS  
PL

## ABSTRACT

Pr<sup>3+</sup> doped strontium fluoride (SrF<sub>2</sub>) was prepared by hydrothermal and combustion methods. The phosphors were characterized by X-ray diffraction (XRD), scanning electron microscope (SEM), X-ray photoelectron spectroscopy (XPS) and Photoluminescence (PL) spectroscopy. XRD patterns indicated that the samples were completely crystallized with a pure face-centred cubic (space group: Fm3m) structure. SEM images showed different morphologies which is an indication that the morphology of the SrF<sub>2</sub>:Pr<sup>3+</sup> phosphor strongly depends on the synthesis procedure. Both the SrF<sub>2</sub>:Pr<sup>3+</sup> samples exhibit blue–red emission centred at 488 nm under a 439 nm excitation wavelength ( $\lambda_{exc}$ ) at room temperature. The emission intensity of Pr<sup>3+</sup> was also found to be dependent on the synthesis procedure. The blue–red emission has decreased with an increase in the Pr<sup>3+</sup> concentration. The optimum Pr<sup>3+</sup> doping level for maximum emission intensity was 0.4 and 0.2 mol% for the hydrothermal and combustion samples, respectively. The reduction in the intensity for higher concentrations was found to be due to dipole–dipole interaction induced concentration quenching effects.

© 2015 Elsevier B.V. All rights reserved.

## 1. Introduction

Pr<sup>3+</sup> is an interesting ion because it has multiple transitions that allows for detailed studies of both radiative and non-radiative mechanisms. Pr<sup>3+</sup> doped materials have been extensively investigated due to its potential use in a variety of applications [1–5]. For phosphor applications, the 4f–4f transitions are the most relevant, especially the <sup>1</sup>D<sub>2</sub> → <sup>3</sup>H<sub>4</sub> red emission from Pr<sup>3+</sup> doped oxide materials [6,7]. Recently, the Pr<sup>3+</sup> ion was found to be a promising co-doped ion in the lanthanide-based luminescent materials to be used for quantum cutting with the Yb ion, which can be used to enhance the solar cell efficiency [1,8]. Quantum cutting with Pr<sup>3+</sup> requires a host material with a lower vibrational energy. Strontium fluoride (SrF<sub>2</sub>) has very small cut-off phonon energy (~350 cm<sup>-1</sup>) and was found to be a good host for the quantum cutting application [1,8].

The SrF<sub>2</sub>:Pr<sup>3+</sup> system has been investigated by several researchers [5,9,10] and the majority reported the photon emission cascade and energy transfer mechanism in SrF<sub>2</sub> doped with Pr<sup>3+</sup> ions (with the main focus on the 4f<sup>n</sup>–4f<sup>n-1</sup>5d emission). The 4f–4f transitions have also been studied, but most of these results have been devoted to the red emission from Pr<sup>3+</sup> doped oxide materials [6,7,11]. On

the other hand, it has been shown that the probability of the multi-phonon relaxation between <sup>3</sup>P<sub>0</sub> and <sup>1</sup>D<sub>2</sub> levels of Pr<sup>3+</sup> significantly decreases as the phonon energy of the host decreased [12]. It has also been observed that the emission intensity of the <sup>3</sup>P<sub>0</sub> state of the Pr<sup>3+</sup> doped host with a small phonon energy decreased with increasing the Pr<sup>3+</sup> concentration. This was attributed to cross-relaxation processes [12–15]. This behavior normally occurs at the smaller average interionic distances between the Pr<sup>3+</sup> ions.

Most investigations on the concentration quenching of Pr<sup>3+</sup> doped crystals have been studied in oxide hosts. The different pathways by which cross-relaxation can take place makes Pr<sup>3+</sup> a challenging ion to study. The low phonon energy of the SrF<sub>2</sub> host may play a key role on the optical properties of the dopant ion. Furthermore, the emission intensities of lanthanide ions in a host were found to be strongly dependent on the condition of the synthesis procedure [8]. This was observed on Pr<sup>3+</sup> co-doped Yb<sup>3+</sup> in SrF<sub>2</sub> where the concentration quenching of both ions at small concentrations reduced the near infrared emission intensity and prevented more quantitative assessment of the quantum cutting efficiency. The SrF<sub>2</sub>:Pr, Yb quantum cutting samples were synthesised by solid state reaction [8]. It is therefore quite meaningful to study the effect of different synthesis techniques on the concentration quenching of Pr<sup>3+</sup> in SrF<sub>2</sub> phosphor. In this paper, the surface and spectral investigation of Pr<sup>3+</sup> doped SrF<sub>2</sub> phosphor powders prepared by using both the hydrothermal and combustion methods

\* Corresponding author.

E-mail address: [Coetsee@ufs.ac.za](mailto:Coetsee@ufs.ac.za) (E. Coetsee).

are studied. The concentration quenching of  $\text{Pr}^{3+}$  for both methods was investigated.

## 2. Experimental

Cubic  $\text{SrF}_2$  nanocrystals doped with  $\text{Pr}^{3+}$  were prepared using hydrothermal and combustion synthesis procedures, as previously described [16,17]. For the hydrothermal synthesis, analytical grade of  $\text{Sr}(\text{NO}_3)_2$ ,  $\text{Pr}(\text{NO}_3)_3 \cdot 6\text{H}_2\text{O}$ ,  $\text{NH}_4\text{F}$ , sodium oleate, oleic acid and ethanol were used without further purification. For a typical synthesis of  $\text{SrF}_2:\text{Pr}^{3+}$ , ethanol, sodium oleate and oleic acid were added simultaneously to an aqueous solution containing  $\text{Sr}(\text{NO}_3)_2$ ,  $\text{NH}_4\text{F}$  and  $\text{Pr}(\text{NO}_3)_3 \cdot 6\text{H}_2\text{O}$ . After 10 min of stirring the milky colloidal solution was transferred to a 125 ml autoclave lined with Teflon and heated at  $180^\circ\text{C}$  for 24 h. The product was collected by centrifugal and washed with water and ethanol. Finally, the product was dried for 24 h in an oven at  $80^\circ\text{C}$ . The as-prepared  $\text{SrF}_2:\text{Pr}^{3+}$  samples did not emit, therefore, they were sintered for 2 h at  $450^\circ\text{C}$ .

In the combustion synthesis, an aqueous solution of  $\text{NH}_4\text{F}$  was added drop wise to a mixture of  $\text{Sr}(\text{NO}_3)_2$ ,  $\text{Pr}(\text{NO}_3)_3 \cdot 6\text{H}_2\text{O}$  and urea, which was used as fuel. The milky solution was collected after thoroughly stirring. Then, the obtained solution was transferred into a porcelain crucible and placed in a furnace at  $500^\circ\text{C}$  until the ignition occurred. Finally, the as-prepared powder was sintered for 2 h at  $700^\circ\text{C}$ .

The phosphors were characterized by X-ray diffraction (XRD) (Bruker Advance D8 diffractometer with  $\text{Cu K}\alpha$  radiation ( $\lambda = 0.154 \text{ nm}$ )) to identify the crystalline structure of the powder. Photoluminescence (PL) and photoluminescence excitation (PLE) spectra were collected using a Cary Eclipse fluorescence spectrophotometer and Horiba scientific (Fluorolog-3) spectrofluorometer equipped with a xenon lamp. The surface morphology was recorded using a Shimadzu Supers-can scanning electron microscope (SEM) model ZU SSX-550. High resolution X-ray photoelectron spectroscopy (XPS) was obtained with a PHI 5000 Versaprobe system. A low energy  $\text{Ar}^+$  ion gun and low energy neutralizer electron gun were used to minimize charging on the surface. A  $100 \mu\text{m}$  diameter monochromatic  $\text{Al K}\alpha$  X-ray beam ( $h\nu = 1486.6 \text{ eV}$ ) generated by a 25 W, 15 kV electron beam was used to analyze the different binding energy peaks. The pass energy was set to 11 eV giving an analyzer resolution  $\leq 0.5 \text{ eV}$ . Multipack version 8.2 software was utilized to analyze the spectra to identify the chemical compounds and their electronic states using Gaussian–Lorentz fits. All measurements were performed at room temperature.

## 3. Results and discussion

Fig. 1(a) depicts the XRD patterns of  $\text{SrF}_2:\text{Pr}^{3+}$  prepared by the hydrothermal and combustion method as well as the standard data for  $\text{SrF}_2$  (card No. 00-086-2418). The strong diffraction peaks indicate that the samples powder is fully crystallized (face-centred cubic with space group:  $\text{Fm}\bar{3}\text{m}$ ). The patterns for doped samples with  $\text{Pr}^{3+}$  are similar to those from the pure  $\text{SrF}_2$  matrix. This indicates that there is no obvious influence of the dopants on the crystalline structure of the host. It can, however, be noticed that doping of  $\text{Pr}^{3+}$  in both methods causes a slight shift to a higher angle with comparison to the standard data (Fig. 1(a)). This can be attributed to the radius difference between  $\text{Pr}^{3+}$  (0.099 nm) and  $\text{Sr}^{2+}$  (0.126 nm) ions, which confirms that  $\text{Pr}^{3+}$  ions are incorporated into the  $\text{SrF}_2$  lattice. The sintering temperature of the as-prepared hydrothermal samples caused a slight variation in the XRD intensities. The reason might be that, the orientation growth of the particles occurred in certain directions. The calculated  $\text{SrF}_2$  lattice parameter is  $(5.778 \pm 0.0025) \text{ \AA}$  and

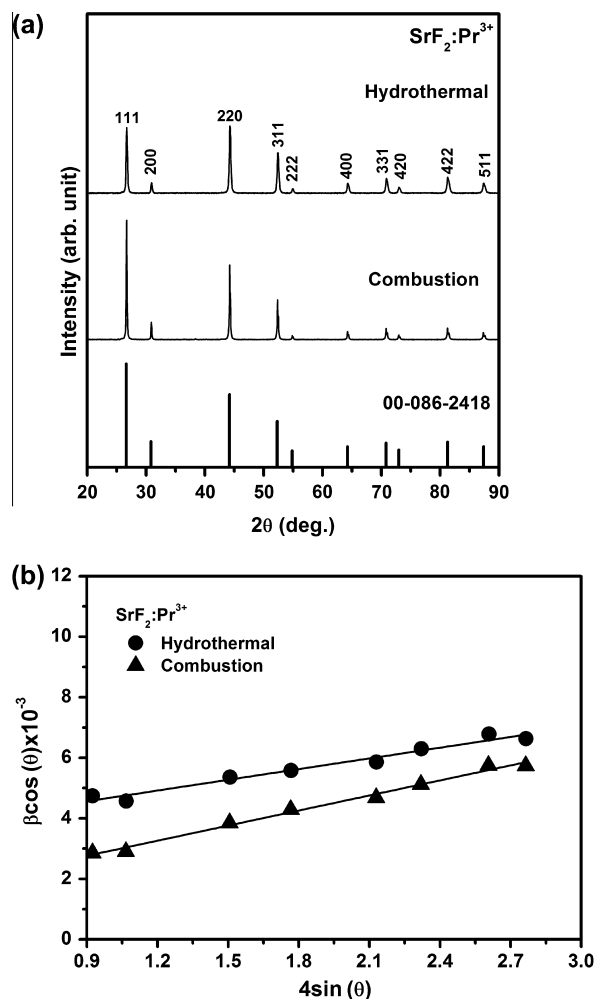


Fig. 1. (a) XRD patterns of  $\text{SrF}_2:\text{Pr}^{3+}$  phosphors; (b) Williamson–Hall plots for  $\text{Pr}^{3+}$  doped  $\text{SrF}_2$  samples for both the hydrothermal and combustion methods.

$(5.775 \pm 0.0054) \text{ \AA}$  for the samples prepared by the combustion and hydrothermal methods, respectively. These results agreed well with reported values [17].

Fig. 1(b) shows Williamson–Hall plots for the combustion and hydrothermal samples, where the peak broadening is dependent on both crystallite size and microstrain. The Williamson–Hall equation is given by  $\beta\cos\theta = K\lambda/S + 4\epsilon\sin\theta$ , where  $\lambda$  is the wavelength of the X-rays (0.154 nm) and  $\beta$  is the full-width at half maximum of the X-ray peak at the Bragg angle  $\theta$ ,  $K$  is a shape factor taken as 0.9,  $S$  is the crystallite size and  $\epsilon$  is the microstrain [18]. The slope of this equation is equal to the microstrain and the crystallite size can be calculated from the intercept ( $K\lambda/S$ ). The microstrain of both the hydrothermal and combustion samples has values approximately of 0.0012 (0.12%) and 0.0017 (0.17%), respectively, showing only very small amount of microstrain in this produced materials. The bigger strain was produced by combustion synthesis, which might be true as the combustion technique requires a higher temperature. The estimated average crystallite size ( $S$ ) of the particles was calculated from both the slope of the William–Hall equation and from the well-known Debye–Scherrer’s equation [19]. These are tabulated in Table 1. This shows that the hydrothermal method produces a smaller particle size.

SEM images were obtained in order to investigate the surface morphology of the synthesized phosphors. Fig. 2 represents the SEM images that were taken from the powders that were prepared by the different synthesis methods ((a) combustion and (b)

**Table 1**

The estimated average crystallite size (*S*) of the particles using the William–Hall and the well-known Debye–Scherrer's equations.

	<i>S</i> using Debye–Scherrer's equation (nm)	<i>S</i> using William–Hall equation (nm)
Hydrothermal	37–41	36
Combustion	56–62	69

hydrothermal). The results indicate different types of morphology. The combustion synthesis produced large number of particles and voids, which may be due to the high temperature reaction during the combustion process. In hydrothermal synthesis fluffy type morphology was formed. These results suggested that the synthesis procedure strongly change the morphology of the SrF<sub>2</sub>:Pr<sup>3+</sup> phosphor.

XPS measurements have been done in order to investigate the chemical, composition and bonding state of the SrF<sub>2</sub>:Pr<sup>3+</sup> phosphors. There was no difference observed in the XPS spectra of the two synthesis methods. Fig. 3 shows the peak fits for the (a) Sr 3d, (b) F 1s and (c) Pr 3d high resolution XPS peaks and (d) the survey scan for SrF<sub>2</sub>:Pr<sup>3+</sup>. The results confirmed the presence of Sr, F, and Pr to their corresponding binding energies. In addition C and O were also observed. The C contamination is attributed to adventitious hydrocarbons which are known to be always present [20]. In a fluoride compound oxygen is considered to be a common impurity [21]. In fact the presence of the O in the sample did not change the structure of the sample (see Fig. 1(a)). Therefore, the O contamination was due to adventitious impurity species in the surface rather than oxygen impurity in the SrF<sub>2</sub> matrix. During the peak fit procedure, the C 1s peak at 284.8 eV was taken as a reference for all charge shift corrections. This is done because the C 1s peak resulted from hydrocarbon contamination and its binding energy generally remains constant, irrespective to the chemical state of the sample. In the peak fit procedure, all the Gaussian percentages were assumed to have a combined Gaussian–Lorentzian shape. The high resolution XPS peak for the Sr 3d showed two individual peaks. These two peaks are assigned to Sr 3d in SrF<sub>2</sub> that originate from the spin–orbit splitting 3d<sub>5/2</sub> (133.52 eV) and 3d<sub>3/2</sub> (135.30 eV), while the F 1s peak is situated at 684.67 eV. The Pr 3d<sub>5/2</sub> signal was comparatively low, which is due to a very low doping concentration of Pr. The high resolution XPS for Pr 3d<sub>5/2</sub> peak consists of two individual peaks, which are assigned to the Pr<sup>3+</sup> peak in SrF<sub>2</sub>:Pr<sup>3+</sup> and a satellite peak that is always present in the Pr 3d spectra [22,23]. These results not only approved the formation of the SrF<sub>2</sub> matrix, but also confirm the presence of the Pr dopant in the material.

Fig. 4(a)–(c) shows the excitation and emission spectra of the SrF<sub>2</sub> phosphor doped with Pr<sup>3+</sup> ions that were prepared by the combustion and the hydrothermal methods. The extra charge of Pr<sup>3+</sup> doped SrF<sub>2</sub> was compensated locally by F<sup>−</sup> ions. All observed excitation and emission bands are similar in both synthesis methods. The excitation spectrum of SrF<sub>2</sub>:Pr<sup>3+</sup> (Fig. 4(a)) was obtained by monitoring the emission centered at 488 nm (<sup>3</sup>P<sub>0</sub> → <sup>3</sup>H<sub>4</sub> transition). The observed excitation bands are similar in both synthesis, which are corresponding to the transitions of <sup>3</sup>H<sub>4</sub> → <sup>3</sup>P<sub>*j*</sub> (*j* = 0, 1, 2) and <sup>1</sup>I<sub>6</sub>. All these bands occurred within the 4f–4f transitions of the Pr<sup>3+</sup> ion [11]. The metastable <sup>3</sup>P<sub>0</sub> energy level depopulated through non-radiative relaxation when any level above <sup>3</sup>P<sub>0</sub> is optically excited. Upon excitation with 439 nm (into the <sup>1</sup>I<sub>6</sub> and <sup>3</sup>P<sub>*j*</sub>, *j* = 0, 1, 2), depopulation from the <sup>1</sup>I<sub>6</sub> and <sup>3</sup>P<sub>1,2</sub> energy bands occurred to the metastable <sup>3</sup>P<sub>0</sub> energy band. Both samples exhibit blue–red emission from the <sup>3</sup>P<sub>0</sub> level. There are at least six luminescent bands that correspond to relaxation from the <sup>3</sup>P<sub>0</sub> emission energy band. These six bands are centered at 488, 524, 605, 638, 715 and 730 nm, which are assigned to the <sup>3</sup>P<sub>0</sub> → <sup>3</sup>H<sub>4</sub>, <sup>3</sup>P<sub>0</sub> → <sup>3</sup>H<sub>5</sub>, <sup>3</sup>P<sub>0</sub> → <sup>3</sup>H<sub>6</sub>, <sup>3</sup>P<sub>0</sub> → <sup>3</sup>F<sub>2</sub>, <sup>3</sup>P<sub>0</sub> → <sup>3</sup>F<sub>3</sub> and <sup>3</sup>P<sub>0</sub> → <sup>3</sup>F<sub>4</sub> transitions, respectively [8]. This demonstrates that the dominant transition in SrF<sub>2</sub> is the <sup>3</sup>P<sub>0</sub> transition. There is also a small peak marked with (S) around 879 nm (Fig. 4(b) and (c)), which is assigned to the second order observation of the excitation wavelength. This band has been previously assigned to the <sup>3</sup>P<sub>0</sub> → <sup>1</sup>G<sub>4</sub> transitions [8], but in this work, we observed that its position changes with the excitation wavelength, which is exactly twice of the excitation wavelength (λ<sub>exc</sub>). The second order observation of the Pr<sup>3+</sup> system has also been previously reported on Pr<sup>3+</sup> doped YF<sub>3</sub> [2]. The actual peak of <sup>3</sup>P<sub>0</sub> → <sup>1</sup>G<sub>4</sub> transition in SrF<sub>2</sub> host is very much weaker and can be clearly seen in the inset of Fig. 4(c). Its position in the fluoride hosts was found around 974 nm, which is well in agreement with our results [24].

Concentration quenching is considered to be a common energy loss mechanism for dopant ions. We therefore have prepared the SrF<sub>2</sub> phosphors doped with different concentrations of Pr<sup>3+</sup> ions. Fig. 5 shows the <sup>3</sup>P<sub>0</sub> → <sup>3</sup>H<sub>4</sub> emission intensity variation as a function of Pr<sup>3+</sup> concentration for combustion and hydrothermal methods. It is worth mentioning that all the samples were carefully synthesized and measured under the same condition for each preparation method so that the Pr<sup>3+</sup> ion emission intensity can be compared. In the combustion method, the PL intensity of the <sup>3</sup>P<sub>0</sub> emission increased until around 0.2 mol% Pr<sup>3+</sup> concentration, whereas in the hydrothermal method it increased from 0.1 up to around 0.4 mol% Pr<sup>3+</sup> concentrations. It then started to decrease systematically as the Pr<sup>3+</sup> concentration increased. This demonstrates that the optimum Pr<sup>3+</sup> doping for maximum luminescence of Pr<sup>3+</sup> doped SrF<sub>2</sub> was about 0.2 and 0.4 mol% for the combustion

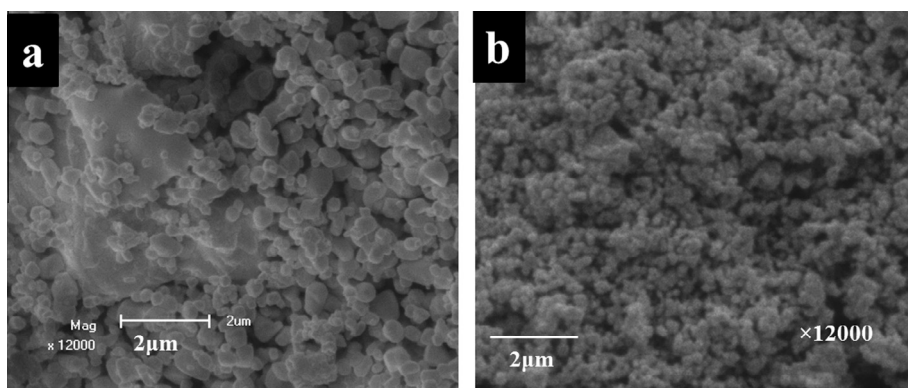


**Fig. 2.** SEM images of SrF<sub>2</sub>:Pr<sup>3+</sup> phosphors prepared by different synthesis methods (a) combustion and (b) hydrothermal.

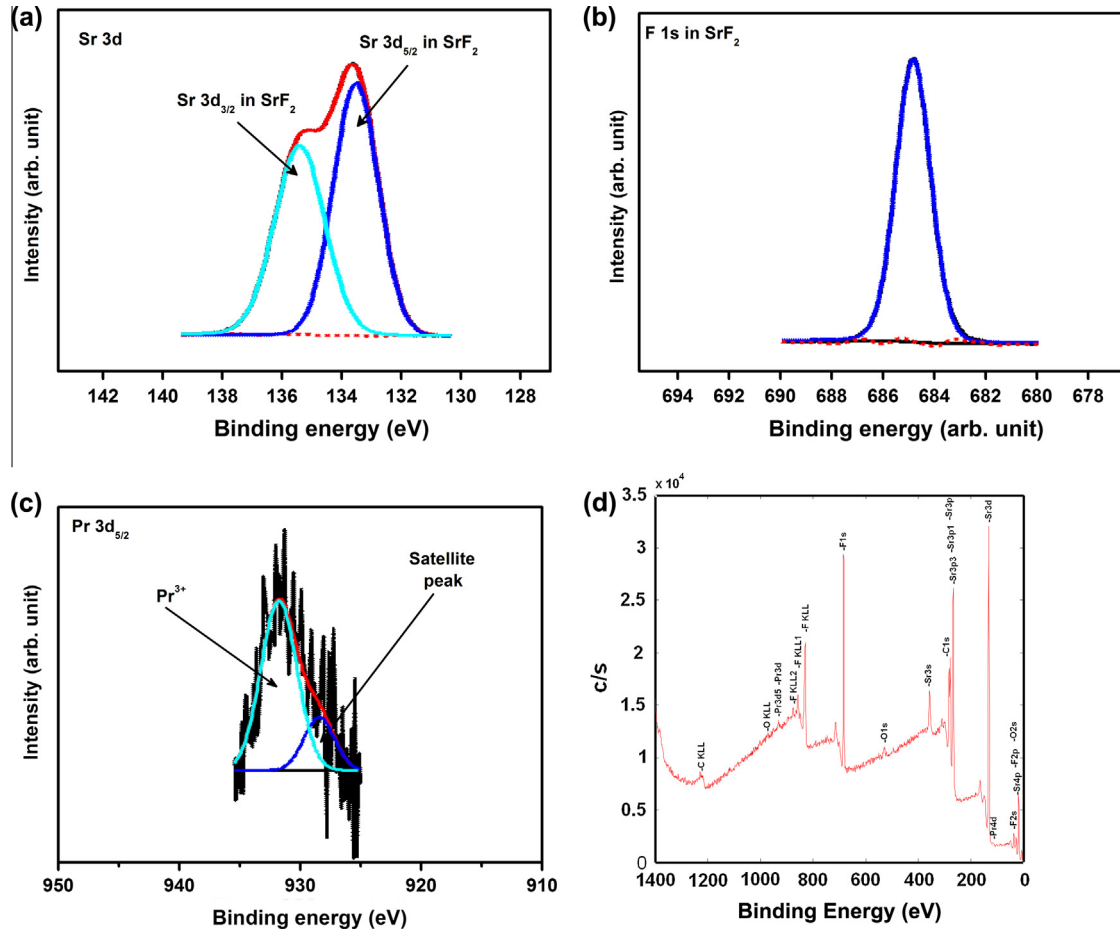


Fig. 3. High resolution XPS peaks of (a) Sr 3d, (b) F 1s, (c) Pr 3d<sub>5/2</sub> and (d) survey scan for SrF<sub>2</sub>:Pr<sup>3+</sup> phosphors.

and hydrothermal samples, respectively. The same behavior was also observed for the other emission bands. When the Pr<sup>3+</sup> ions concentration increases, the Pr<sup>3+</sup>–Pr<sup>3+</sup> distance decreases. This causes non-radiative energy transfers between Pr<sup>3+</sup> ions. Therefore, the emission intensity strongly depends on the distance between Pr<sup>3+</sup> ions. Thus, the difference in the intensity optimization between the synthesis methods can be associated to the distance between nearby Pr<sup>3+</sup> ions. This assumption is drawn from the knowledge that the lanthanide ions form clusters in SrF<sub>2</sub> because charge compensation is required when Sr<sup>2+</sup> is substituted by Pr<sup>3+</sup> ions [25,26]. The Pr<sup>3+</sup> ions form less clustering in the hydrothermal samples relative to that in the combustion samples. This makes the energy transfer between Pr<sup>3+</sup> ions in combustion samples more effective than in hydrothermal samples. However, the non-radiative emission from <sup>3</sup>P<sub>0</sub> level normally occurs through two different processes: relaxation by multi-phonon emission to the <sup>1</sup>D<sub>2</sub> level, or cross-relaxation between Pr<sup>3+</sup> pairs. As it is mentioned earlier the probability of the multi-phonon process significantly reduces as the phonon energy of the host decreases [12]. However, the energy difference between <sup>3</sup>P<sub>0</sub> and <sup>1</sup>D<sub>2</sub> is around 3500 cm<sup>-1</sup> and the energy cut-off of the SrF<sub>2</sub> is about 350 cm<sup>-1</sup>. This means that ten phonons are required to bridge the energy gap. It is well known that when the number of required phonons exceeded 5, the possibility of multi-phonon relaxation to occur is low. Hence, the multi-phonon relaxation processes for the <sup>3</sup>P<sub>0</sub> and <sup>1</sup>D<sub>2</sub> levels can be considered negligible. Therefore, the <sup>3</sup>P<sub>0</sub> emission quenching might occur due to the cross-relaxation mechanism between the nearby Pr<sup>3+</sup> ions as a results of clustering effects.

It is necessary to describe the type of interaction that is responsible for the non-radiative energy transfer process between the Pr<sup>3+</sup> ions. According to Dexter's theory [27], if the energy transfer occurs between the same sorts of activators, the strength of the multipolar interaction can be determined from the change of the emission intensity with concentration ions as follow:

$$\frac{I}{C} = \kappa \left(1 + \beta(C)^{Q/3}\right)^{-1} \quad (1)$$

where  $C$  is the activator concentration;  $Q = 6, 8, 10$  for dipole–dipole, dipole–quadrupole, quadrupole–quadrupole interactions, respectively; and  $\kappa$  and  $\beta$  are constant for the same excitation conditions for a given host material.

At a concentration  $C$  higher than the critical quenching concentration  $C_c$ , Eq. (1) can be approximated to Eq. (2) below for  $\beta(C)^{Q/3}$  [28];

$$\frac{I}{C} = \frac{\kappa'}{\beta(C)^{Q/3}} \quad (2)$$

where  $\kappa'$  is constant and  $C$  is the activator concentration greater than  $C_c$ . Fig. 6 represents  $\log I/C$  as a function of  $\log C$ . It can be seen that the dependence of  $\log I/C$  versus  $\log C$  is linear for both techniques and the line slopes are  $-2.006$  and  $-2.05759$  for the combustion and hydrothermal, respectively. Therefore the value of  $Q$  for both techniques is approximately equal to 6, which indicates that the dipole–dipole interaction between Pr<sup>3+</sup> ions is the mechanism that is responsible for the concentration quenching in the SrF<sub>2</sub>:Pr<sup>3+</sup> phosphor. The dipole–dipole interactions have also been

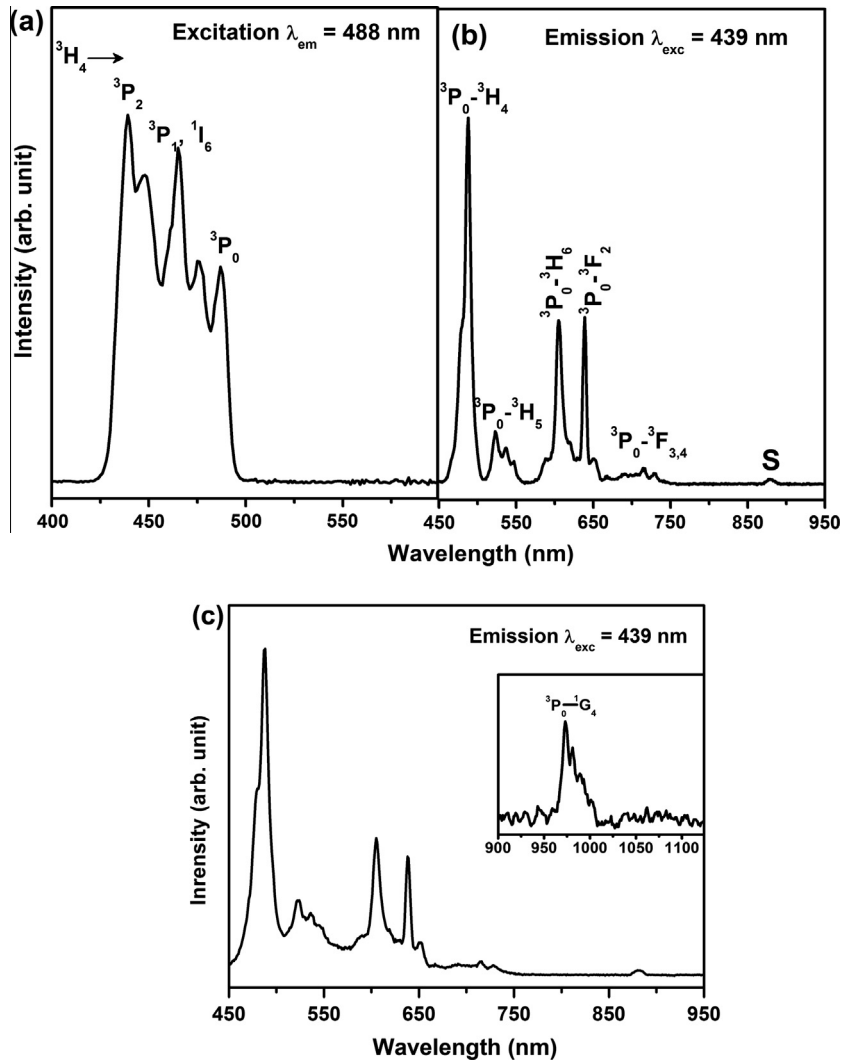


Fig. 4. Excitation and emission spectra of  $\text{SrF}_2:\text{Pr}^{3+}$  at different synthesis methods, (a) excitation and (b) emission spectrum for combustion method, (c) emission spectrum for hydrothermal method. The inset shows the weak  ${}^3\text{P}_0 \rightarrow {}^1\text{G}_4$  transition band of Pr.

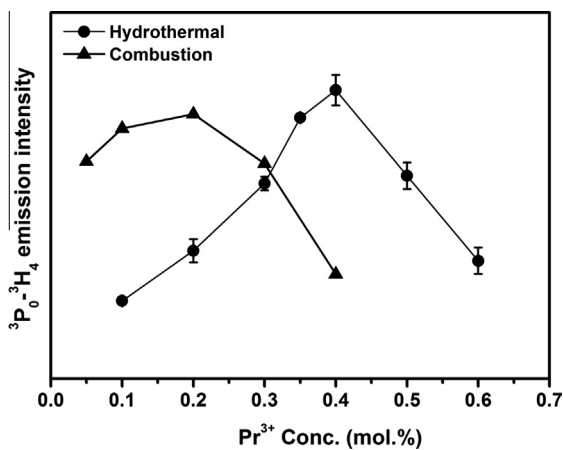


Fig. 5. Variation of the  $\text{Pr}^{3+}$  emission intensity as a function of the  $\text{Pr}^{3+}$  concentration. The vertical lines represent the error bars.

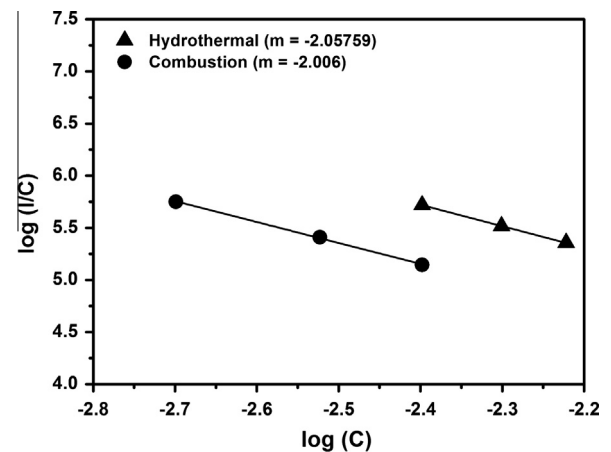


Fig. 6. The curve of  $\log(I/C)$  vs.  $\log(C)$  in  $\text{SrF}_2:\text{Pr}^{3+}$  phosphors.

reported previously to describe the interaction between  $\text{Pr}^{3+}$  ions in  $\text{LaF}_3$  and  $\text{BaTa}_2\text{O}_6$  crystals [29,30]. Such information could be important for the optimization of the  $\text{Pr}^{3+}$  concentration in nano-crystalline materials for certain applications.

#### 4. Conclusion

The  $\text{SrF}_2:\text{Pr}^{3+}$  powder was prepared by hydrothermal and combustion methods. The XRD patterns showed strong and sharp

diffraction peaks for both samples, which indicate that the powders were completely crystallized with a pure face-centred cubic (space group: Fm3m) structure. A comparison between these two methods showed that the calculated particle sizes are smaller for the hydrothermal technique. XPS confirms the presence of Sr, F and Pr materials on the host matrix. It was found that both samples exhibit blue–red emission under 439 nm from 4f–4f excitation at 425 to 500 nm. The optimum Pr<sup>3+</sup> doping level for maximum emission intensity was 0.4 and 0.2 mol% for the hydrothermal and combustion samples, respectively. The reduction of Pr<sup>3+</sup> emission intensity was a result of the Pr<sup>3+</sup> clustering in SrF<sub>2</sub> due to charge compensation. The dipole–dipole interaction between the nearby Pr<sup>3+</sup> ions is responsible for the concentration quenching of Pr<sup>3+</sup> intensity in the SrF<sub>2</sub>:Pr<sup>3+</sup> crystal.

### Acknowledgments

This work is based on the research supported by the South African Research Chairs Initiative of the Department of Science and Technology and National Research Foundation of South Africa. The financial assistance of the National Research Foundation (NRF) and the Cluster program of the University of the Free State towards this research is hereby acknowledged.

### References

- [1] B.M. Van der Ende, L. Aarts, A. Meijerink, *Phys. Chem. Phys. Chem.* 11 (2009) 11081.
- [2] A. Srivastava, S.J. Duclos, *Chem. Phys. Lett.* 275 (1997) 453.
- [3] M.A. Gusowski, H.C. Swart, L.S. Karlsson, M.G. Trzebiatowska, *Nanoscale* 4 (2012) 541.
- [4] A.I. Voloshin, N.M. Navaleev, V.P. Kazakov, *J. Lumin.* 93 (2001) 199.
- [5] N. Kristianpoller, D. Weiss, R. Chen, *Radiat. Meas.* 38 (2004) 719.
- [6] P. Boutinaud, M. Dubois, A.P. Vink, R. Mahiou, *J. Lumin.* 111 (2005) 69.
- [7] P.J. Deren, R. Pazik, W. Strek, P. Boutinaud, R. Mahiou, *J. Alloys Comp.* 451 (2008) 595.
- [8] B.M. Van der Ende, L. Aarts, A. Meijerink, *Adv. Mater.* 21 (2009) 3037.
- [9] E. Radzhabov, *J. Lumin.* 129 (2009) 1581.
- [10] R. Shendrik, E. Radzhabov, *IEEE Trans. Nucl. Sci.* 9499 (2012) 1.
- [11] L.L. Noto, S.S. Pitale, M.A. Gusowski, J.J. Terblans, O.M. Ntwaeaborwa, H.C. Swart, *Powder Technol.* 237 (2013) 141.
- [12] R. Naccache, F. Vetrone, A. Speghnini, M. Bettinelli, J.A. Capobianco, *J. Phys. Chem. C* 112 (2008) 7750.
- [13] R. Balda, J. Fernandez, I.S. Ocariz, M. Voda, A.J. Garcia, *Phys. Rev. B* 59 (1999) 9972.
- [14] Q.J. Chen, W.J. Zhang, X.Y. Huang, G.P. Dong, M.Y. Peng, Q.Y. Zhang, *J. Alloys Comp.* 513 (2012) 139.
- [15] J. Collins, M. Geen, M. Bettinelli, B. Di Bartolo, *J. Lumin.* 132 (2012) 2626.
- [16] J. Sun, J. Xian, H. Du, *Appl. Surf. Sci.* 257 (2011) 3592.
- [17] N. Rakov, R.B. Guimaraes, D.F. Franceschini, G.S. Maciel, *Mater. Chem. Phys.* 135 (2012) 317.
- [18] W.A.I. Tabaza, H.C. Swart, R.E. Kroon, *J. Lumin.* 148 (2014) 192.
- [19] C. Oprea, V. Ciupina, G. Prodan, *Romanian J. Phys.* 53 (2008) 223.
- [20] R.E. Kroon, H.C. Swart, O.M. Ntwaeaborwa, H.A.A. Seed Ahmed, *Physica B* 439 (2014) 83.
- [21] J.T. van Wijngaarden, S. Scheidelaar, T.J.H. Vlugt, M.F. Reid, A. Meijerink, *Phys. Rev. B* 81 (2010) 155112.
- [22] H. Ogasawara, A. Kotani, R. Potze, G.A. Sawatzky, B.T. Thole, *Phys. Rev. B* 44 (1999) 5465.
- [23] J. Gurgul, M.T. Rinke, I. Schellenberg, R. Pottgen, *Solid State Sci.* 17 (2013) 122.
- [24] A. Guille, A. Pereira, G. Breton, A. Bensalah-ledoux, B. Moine, *J. Appl. Phys.* 111 (2012) 043104.
- [25] P.J. Bendall, C.R.A. Catlow, J. Corish, P.W.M. Jacobs, *J. Solid State Chem.* 51 (1988) 159–169.
- [26] D.R. Tallent, D.S. Moore, J.C. Wright, *J. Chem. Phys.* 67 (1977) 2897–2907.
- [27] D.L. Dexter, *J. Chem. Phys.* 21 (1953) 836.
- [28] D. Wang, Q. Yin, Y. Li, M. Wang, *J. Lumin.* 97 (2002) 1.
- [29] G.P. Morgan, D.L. Huber, W.M. Yen, *J. DE Physique* 46 (1985) C7–25.
- [30] M. Ilhan, R. Samur, H. Demiref, F. Mindivan, *Metalurgija* 54 (2015) 407–410.